Supporting Information for

# Competitive Redox Chemistries in Vanadium Niobium Oxide for Ultrafast and Durable Lithium Storage

Xiaobo Ding[1], Jianhao Lin[1], Huiying Huang[1], Bote Zhao[1], Xunhui Xiong[1,*]

[1]School of Environment and Energy, Guangdong Provincial Key Laboratory of Advanced Energy Storage Materials, South China University of Technology, Guangzhou, 510640, P. R. China

*Corresponding author. E-mail: esxxiong@scut.edu.cn (Xunhui Xiong)

## Supplementary Figures and Tables

**Table S1** Cycle performances of $Nb_2O_5$ anodes in other reports

| Cycle test at low current denstiy | | | | | Cycle test at high current denstiy | | | | |
|---|---|---|---|---|---|---|---|---|---|
| Name | Cycle number | Current density (A $g^{-1}$) | Initial capacity (mAh $g^{-1}$) | Retention | Cycle number | Current density (A $g^{-1}$) | Initial capacity (mAh $g^{-1}$) | Retention | Reference |
| H-$Nb_2O_5$ | 100 | 0.2 | 235 | 74.6% | / | / | / | / | [S1] |
| 3DOM $Nb_2O_5$ | / | / | / | / | 100 | 2 | 138 | 90.0% | [S2] |
| T-$Nb_2O_5$@C | 1000 | 0.1 | / | 82.2% | / | / | / | / | [S3] |
| T-$Nb_2O_5$@CC | 1000 | 1 | | 86.0% | 1000 | 2 | / | 85.0% | [S4] |
| $Nb_2O_5$ belt | 50 | 0.1 | 200 | 88.5% | 200 | 1 | 125 | 76.6% | [S5] |
| Wired H-$Nb_2O_5$ | 200 | 0.1 | 160 | 75.0% | / | / | / | / | [S6] |
| $Nb_2O_5$-600 | / | / | / | / | 2000 | 1 | / | 85.0% | [S7] |
| T-$Nb_2O_5$/rGO | 100 | 0.1 | 227 | 72.6% | / | / | / | / | [S8] |
| $Nb_2O_5$ | / | / | / | / | 100 | 1 | / | 85.0% | [S9] |
| $Nb_2O_5$@$NbO_2$ | 900 | 0.2 | | 81.0% | / | / | / | / | [S10] |
| $Nb_2O_5$@C/rGO | 300 | 0.1 | 221 | 85.6% | / | / | / | / | [S11] |
| $Nb_2O_5$ NPs | / | / | / | / | 1000 | 1 | / | 88.0% | [S12] |
| YS-$Nb_2O_5$ | 200 | 0.1 | 205 | 85.30 % | / | / | / | / | [S13] |
| N-NbOC | 1100 | 0.5 | / | 81.0% | / | / | / | / | [S14] |
| $Nb_2O_5$/C | 100 | 0.1 | 559.8 | 43.9% | 300 | / | | | [S15] |
| T-$Nb_2O_5$/CNTs | 500 | 2 | / | 83.0% | 500 | 10 | / | 80.0% | [S16] |
| NC-$Nb_2O_5$ | / | / | / | / | 1000 | 2 | 196 | 83.0% | [S17] |
| T-$Nb_2O_5$ NRs | 270 | 0.1 | 257 | 62.3% | 4000 | 0.5 | 226 | 40.7% | [S18] |
| M-$Nb_2O_5$ | 1000 | 0.2 | 160 | 82.3% | / | / | / | / | [S19] |

| | | | | | | | | | |
|---|---|---|---|---|---|---|---|---|---|
| $Nb_2O_5$@C | 500 | 0.1 | / | 72.0% | / | / | / | / | [S20] |
| TT-$Nb_2O_5$ | / | / | / | / | 1000 | 1 | 103 | 80.7% | [S21] |
| $Nb_2O_5$-C-rGO | / | / | / | / | 1500 | 1 | 192 | 76.6% | [S22] |
| NbW-3/MXene | / | / | / | / | 500 | 1 | / | 59.8% | [S23] |
| H-$Nb_2O_5$ | 100 | 0.05 | 260 | 73.2% | / | / | / | / | [S24] |
| CN-NbO | 550 | 0.1 | 340 | 79.4% | | 1 | 230 | 71.3% | [S25] |
| $Nb_2O_5$ NC | 190 | 0.1 | 224 | 87.0% | 2000 | 2 | 151 | 66.9% | [S26] |
| T-$Nb_2O_5$ | 100 | 0.2 | 184 | 63.5% | 200 | 1 | 92 | 65.2% | [S27] |
| T-$Nb_2O_5$ | 50 | 0.05 | 200 | 47.5% | / | / | / | / | [S28] |
| T-$Nb_2O_5$@C | 1000 | 1 | 110 | 74.5% | / | / | / | / | [S29] |
| T-$Nb_2O_5$/rGO | / | / | / | / | 3000 | 5 | 200 | 80 % | [S30] |
| $Nb_2O_{5-x}$ | 200 | 0.2 | 203.4 | 94% | 1000 | 2 | 159 | 74.8% | [S31] |
| $Nb_2O_5$-5mM | 100 | 0.2 | 285 | 88.4% | / | / | / | / | [S32] |
| CNF/NbO | 100 | 0.2 | 619.2 | 58.3 | / | / | / | / | [S33] |
| $Nb_2O_5$ | 200 | 1 | 105 | 94% | 200 | 2 | 70 | 92% | [S34] |
| N- $Nb_2O_5$ | 100 | 0.1 | / | 83% | 1000 | 1 | / | 70.5% | [S35] |
| N-$Nb_2O_5$ | / | / | / | / | 1000 | 2 | / | 90.1% | [S36] |
| $Nb_2O_5$-750 | 200 | 0.2 | 310 | 87% | 800 | 1 | / | 52% | [S37] |
| $Nb_2O_5$@NC | / | / | / | / | 2900 | 2 | / | 43% | [S38] |

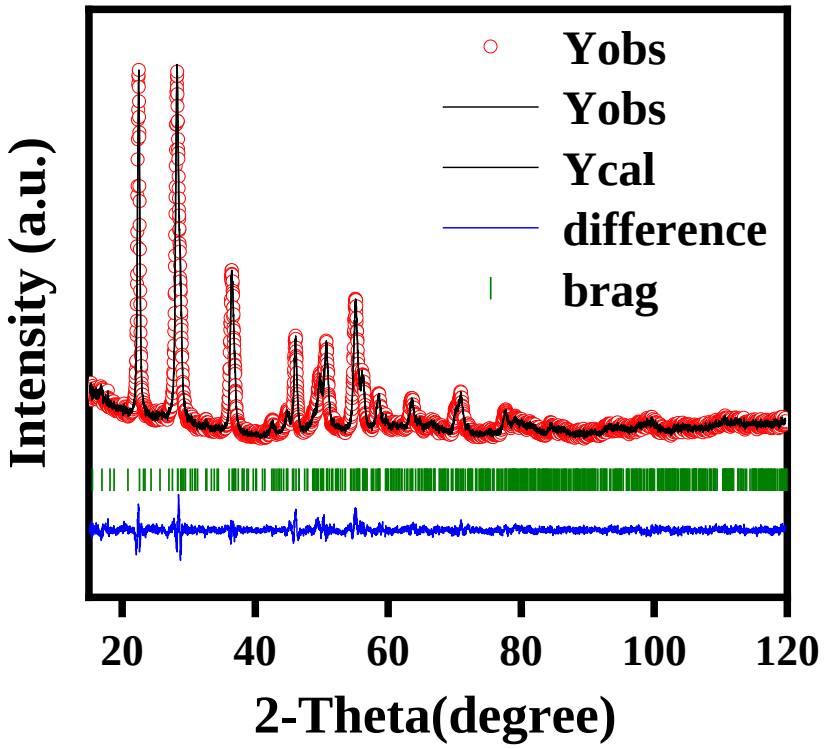


**Fig. S1** Rietveld refinement pattern of T-$Nb_2O_5$

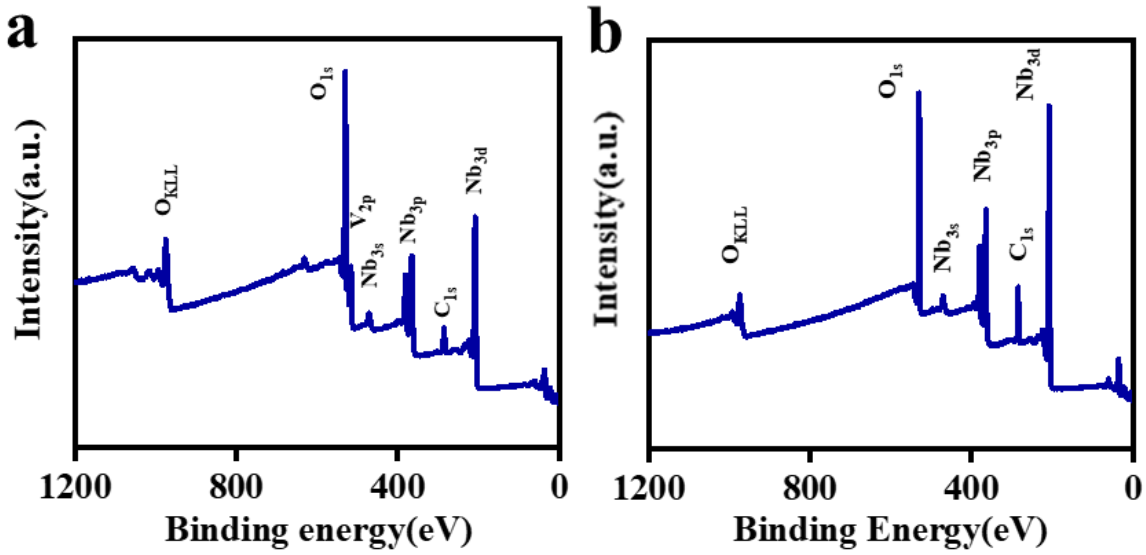


**Fig. S2** XPS spectra of **a** $VNbO_4$. **b** T-$Nb_2O_5$

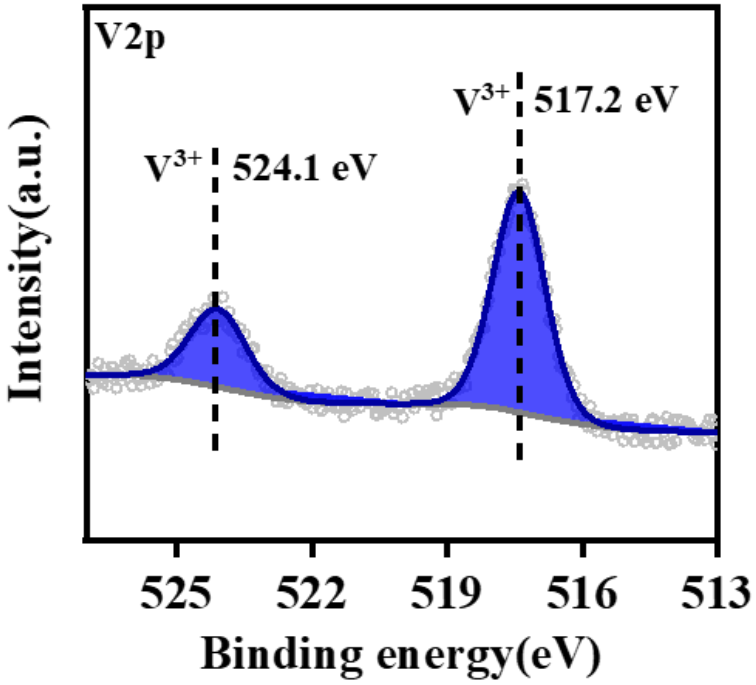


**Fig. S3** Core-level V 2p XPS spectra of $VNbO_4$

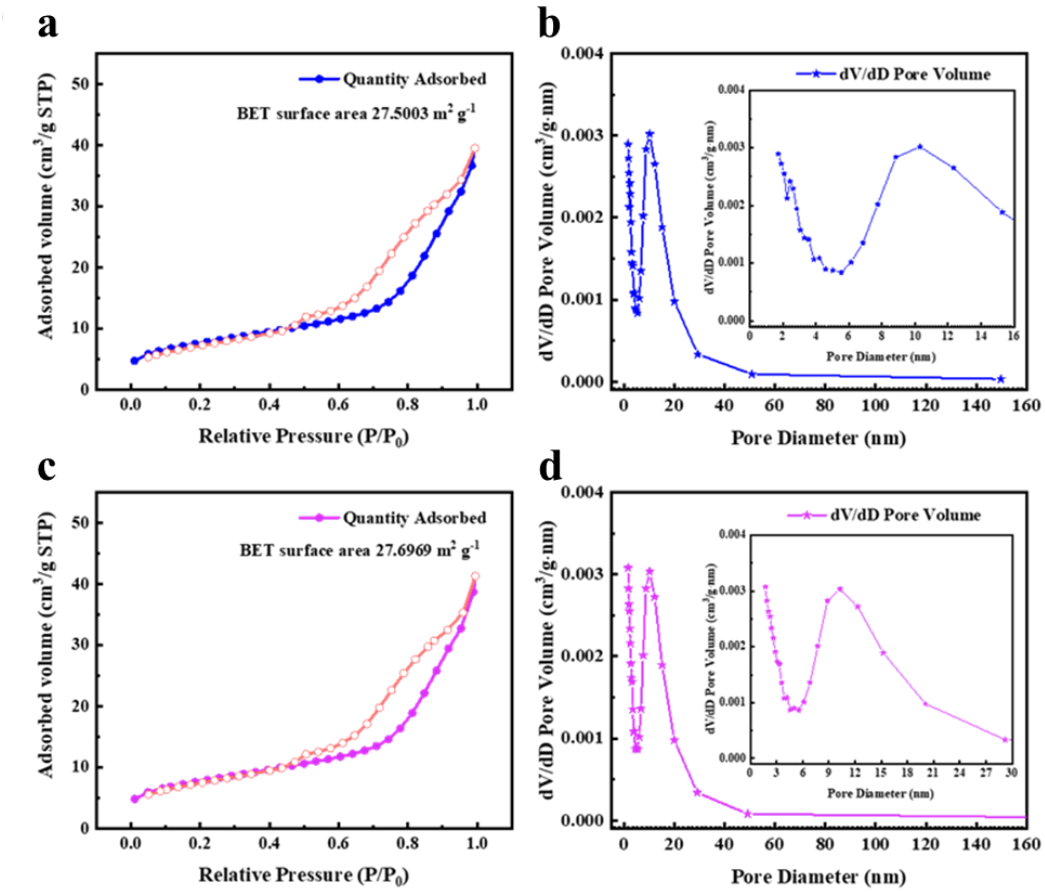


**Fig. S4** $N_2$ adsorption–desorption isotherms of and the pore size distribution. **a** and **b** T-$Nb_2O_5$, **c** and **d** $VNbO_4$

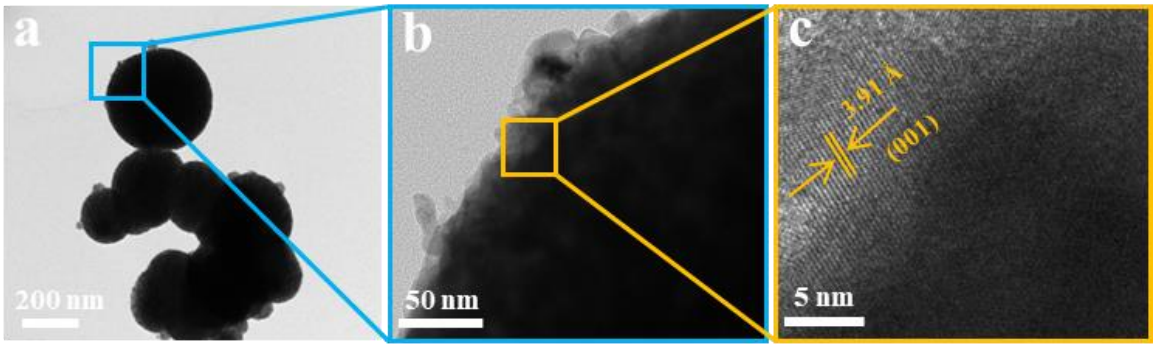


**Fig. S5 a** and **b** TEM images of T-$Nb_2O_5$. **c** HRTEM image of T-$Nb_2O_5$

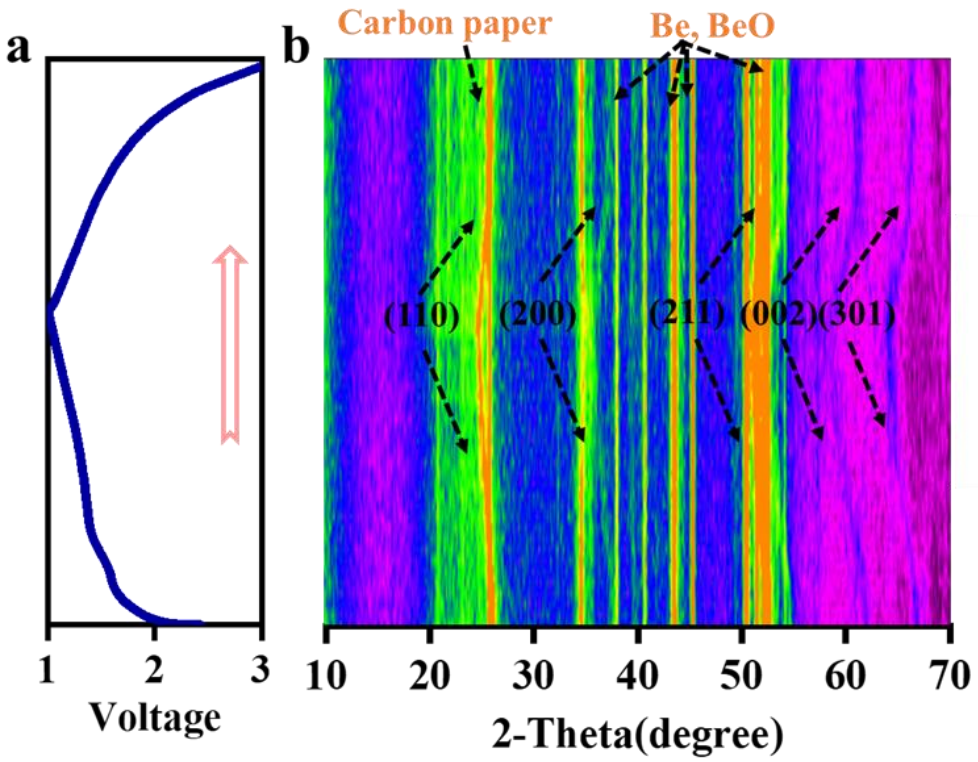


**Fig. S6** Lithium storage mechanism and structure evolution of $VNbO_4$. **a** Electrochemistry profile corresponding to *in-situ* XRD test. **b** The 2D contour of *in-situ* XRD pattern at different lithiation/delithiation states of initial cycle in potential range of 1.0-3.0 V

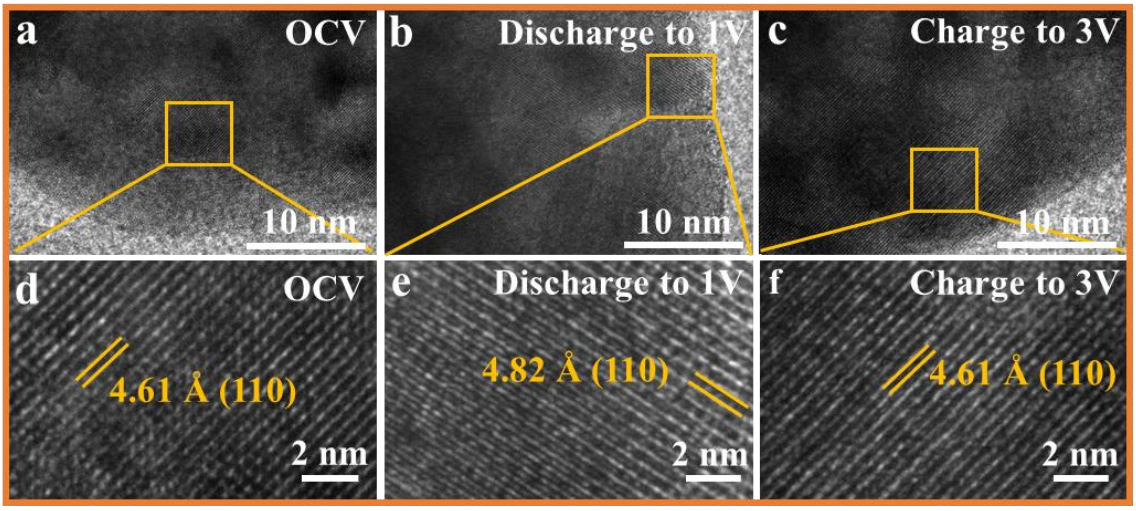


**Fig. S7 a-c** *Ex-situ* TEM images of $VNbO_4$ at different lithiation/delithiation states. **d-f** *Ex-situ* HRTEM images of $VNbO_4$ at different lithiation/delithiation states

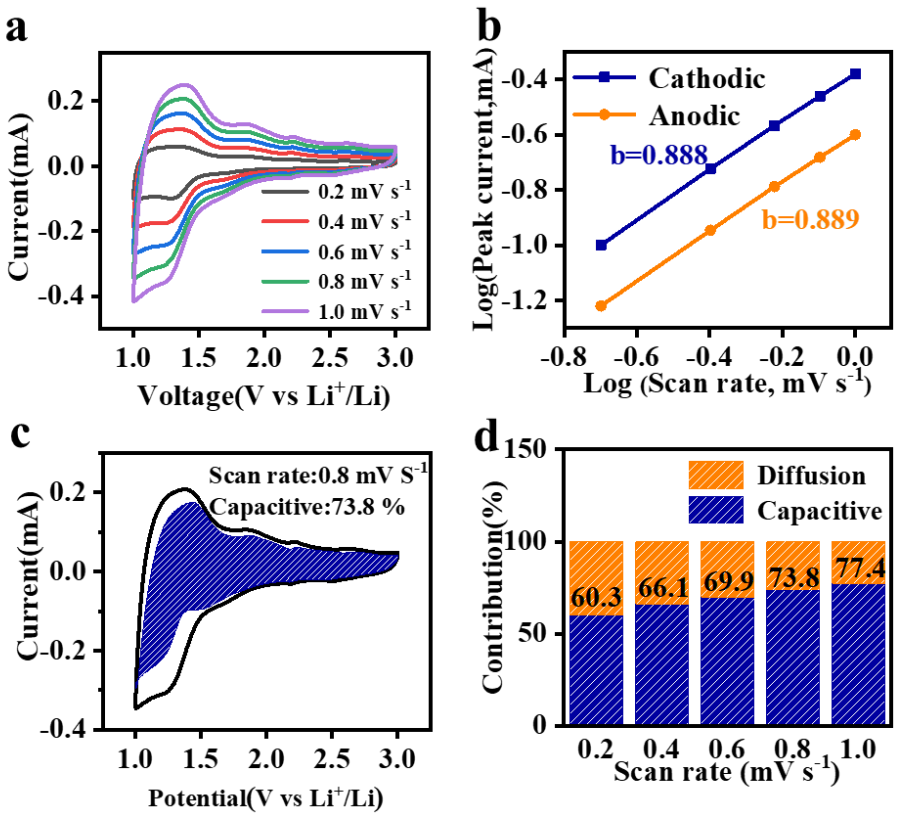


**Fig. S8** The charge-storage behavior of $VNbO_4$ anode. **a** CV curves at different sweep rates. **b** Normalized reduction and oxidation peak currents. **c** Pseudo capacitance fitting pattern of all samples at sweep rate of 0.8 mV $s^{-1}$. **d** Pseudo capacitance contribution

The kinetics of $VNbO_4$ in electrochemical lithium storage can be studied by cyclic voltammetry. Figure S8a shows the CV curves at different sweep rates. The area enclosed by CV curve increasing with the sweep rate, while the voltage values corresponding to peak currents does not change significantly. The following formula was employed to explain the relationship between current values and sweep rates. The *i*, *v* values are respectively corresponding to current value (A), sweep rate (mV $s^{-1}$) while a, b are variable factors.

$$i = av^b \tag{S1}$$

The b value could be obtained to judge the electrochemical behavior of $VNbO_4$-18 after fitting the CV curves at all sweep rate (Figure S8b). Obviously, the obtained b values (0.888 and 0.889) of redox process represent the pseudo capacitive charge storage mechanism controlled by surface of material. In addition, the contribution of pseudo capacitance could be fitted by the following equation. The *i* and *v* values are respectively corresponding to current on selected voltage and the sweep rate, while $k_1$ and $k_2$ are variable factors.

$$i = k_1 v + k_2 v^{1/2} \tag{S2}$$

The fitting results of CV curve with sweep rate of 0.8 mV $s^{-1}$ and the contribution of pseudo capacitance at different sweep rates are shown in Figure S8c and d, indicating that $VNbO_4$ has a surface-controlled pseudo capacitance behavior kinetics.

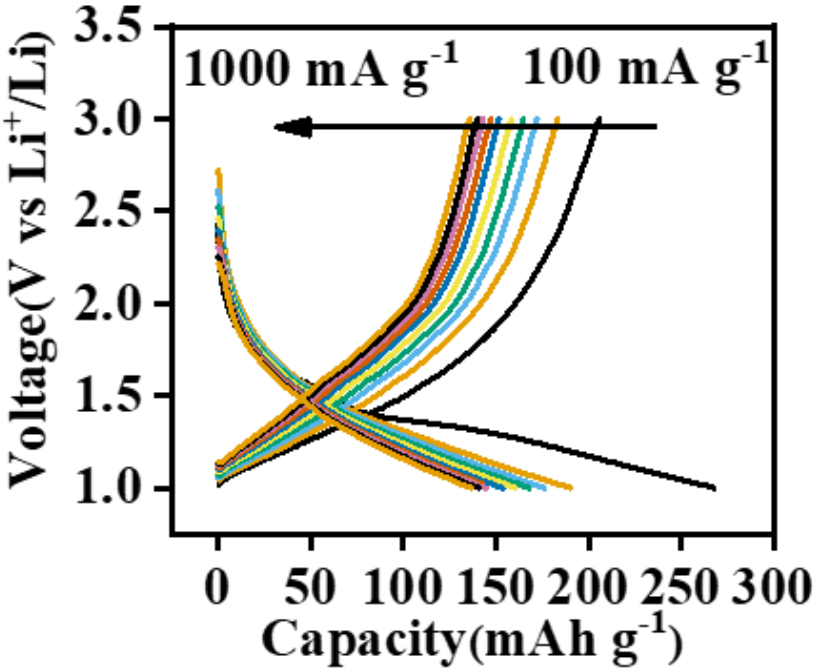


**Fig. S9** Charge-discharge profiles of $VNbO_4$ at different current density

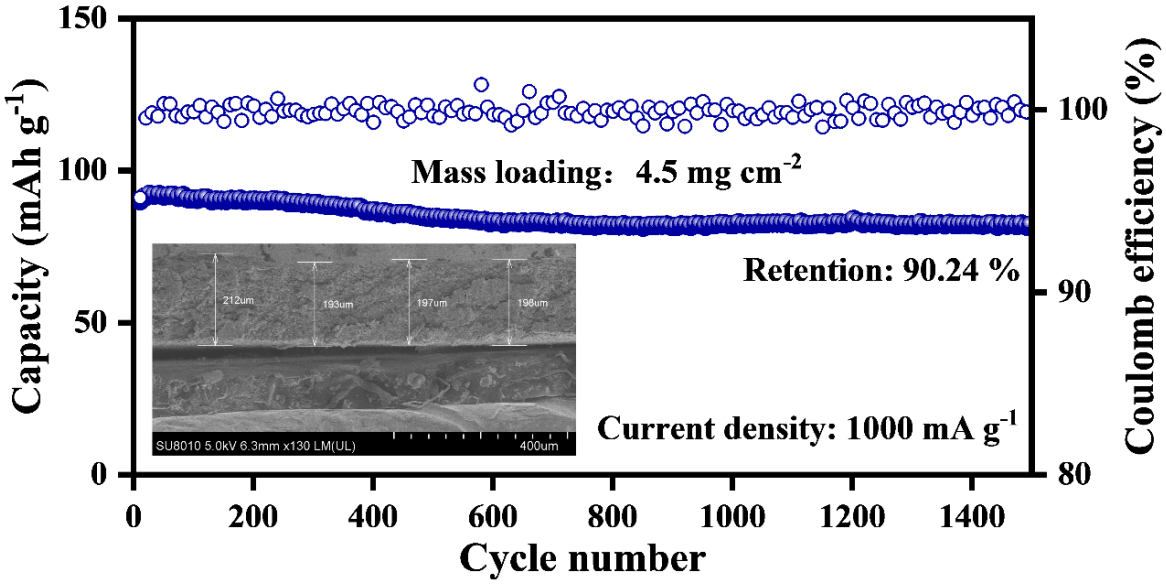


**Fig. S10** Cycle performance of $VNbO_4$ electrode at 1.0 A $g^{-1}$ with mass loading of 4.5 mg $cm^{-2}$ (The inset image shows the cross-section of the electrode)

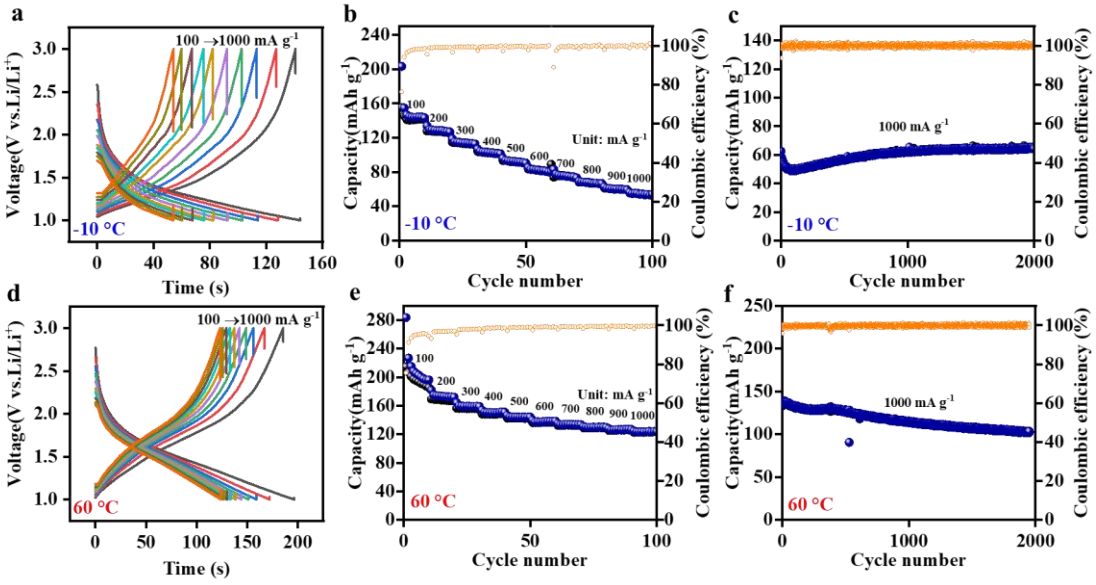


**Fig. S11 a** Charge-discharge profiles, **b** rate performance of $VNbO_4$ at different current density of $VNbO_4$ at -10 °C. **c** Cycle performance of $VNbO_4$ at current density of 1.0 A $g^{-1}$ at -10 °C. **d** Charge-discharge profiles, **e** rate performance of $VNbO_4$ at different current density of $VNbO_4$ at 60 °C. **f** Cycle performance of $VNbO_4$ at current density of 1.0 A $g^{-1}$ at 60 °C

In order to study the electrochemical performance of $VNbO_4$ in a wide temperature range, constant current charge/discharge tests were carried out at -10 °C and 60 °C, respectively (Figure S11). Figure S11a shows the discharge/charge profiles under different current densities at -10 °C. The result shows that the material experienced more obvious polarization than room temperature, which is due to the slow $Li^+$ migration kinetics caused by viscous electrolyte at low temperature. The rate performance test shows that $VNbO_4$ delivered the initial charge capacity 159.2 mAh $g^{-1}$ at 100 mA $g^{-1}$ with coulomb efficiency of 77.2 %. When the current density increases to 1000 mA $g^{-1}$, $VNbO_4$ still delivered a high capacity of 59.2 mAh $g^{-1}$ (Figure S11b). Although the rate capacity had a significant attenuation compared with that at room temperature, which due to the low $Li^+$ diffusion rate at low temperature as well as the high transfer charge impedance, but it is still satisfactory overall, especially considering the test was carried out at such extreme low temperature conditions. The cycle performance at a current density of 1000 mA $g^{-1}$ is shown in Figure S11c. After 2000 cycles, the capacity retention rate of $VNbO_4$ was 102.1%. This increase in capacity can be attributed to the slow activation process at low temperature. When the electrochemical test was carried out at 60 ° C, the polarization degree of the material did not change significantly compared with that at room temperature (Figure S11d). The rate performance test results show that the initial discharge/charge capacity (283.5 mAh $g^{-1}$ and 221.2 mAh $g^{-1}$) of the material was higher than that at room temperature, which can be explained by the enhanced $Li^+$ diffusion ability at high temperature, so that the extra $Li^+$ could insert in bulk of electrode (Figure S11e). However, the coulomb efficiency of the previous cycles was low, due to the formation of thick SEI film caused

by the violent reaction between electrolyte and material surface at high temperature. At the current density of 1000 mA $g^{-1}$, the capacity retention rate after 2000 cycles was 77.8 % (Figure S11f). The cycle stability was slightly worsen compared with that at room temperature, which can be explained by the crystal rupture caused by the accumulated stress of excessive lithium insertion. In conclusion, the wide temperature range test results show that $VNbO_4$ still shows good electrochemical characteristics at both -10 °C and 60 °C , indicating that this new material has high application potential at extreme temperatures.

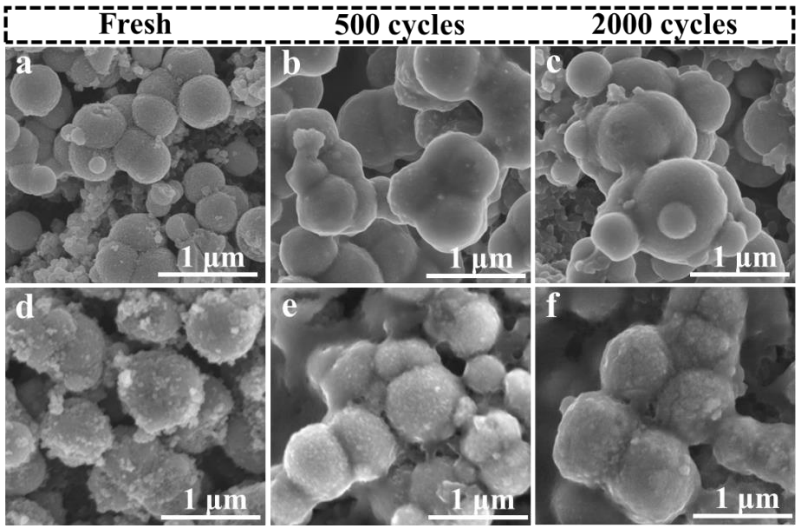


**Fig. S12 a-c** SEM images of $VNbO_4$ at different cycles. **d-f** SEM images of T-$Nb_2O_5$ at different cycles

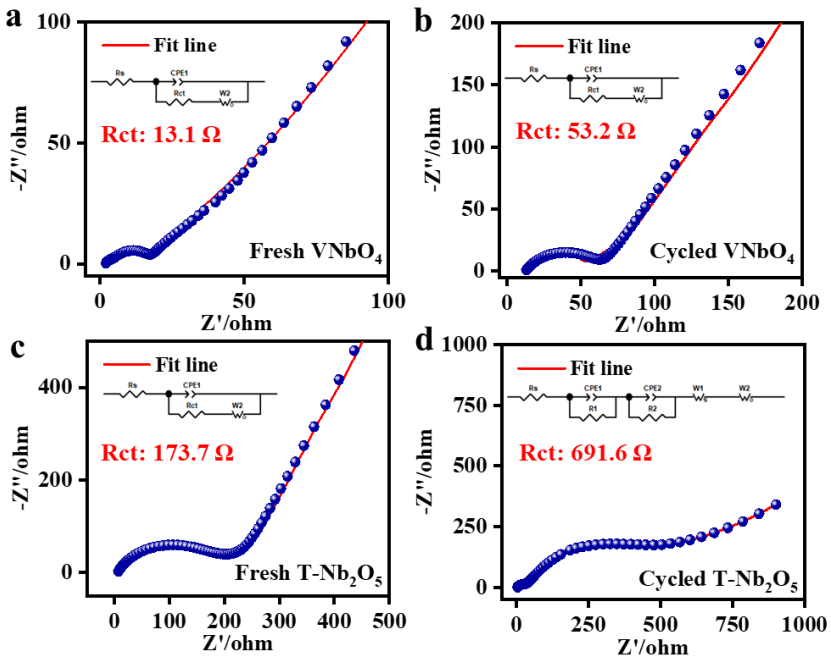


**Fig. S13** Nyquist plots and the fitting results of all samples. **a** Fresh $VNbO_4$. **b** Cycled $VNbO_4$. **c** Fresh T-$Nb_2O_5$. **d** Cycled T-$Nb_2O_5$

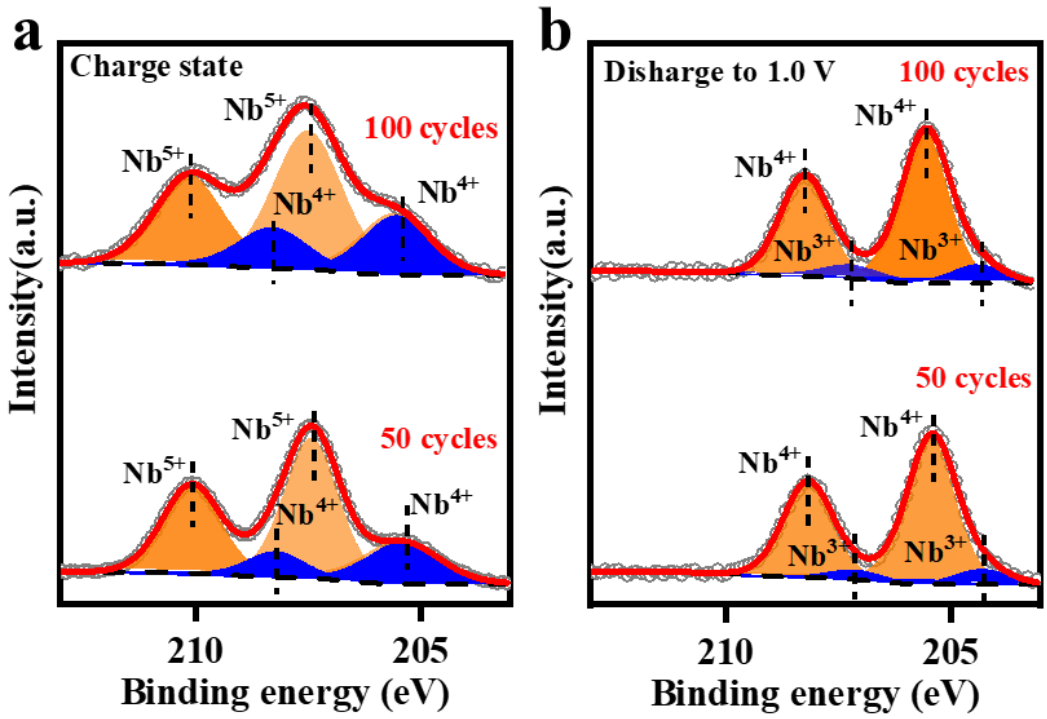


**Fig. S14** The Nb 3d orbit XPS spectra of T-$Nb_2O_5$ electrode at **a** charge state and **b** discharge sate in the 50$^{th}$ and 100$^{th}$ charge-discharge process at 1 A $g^{-1}$

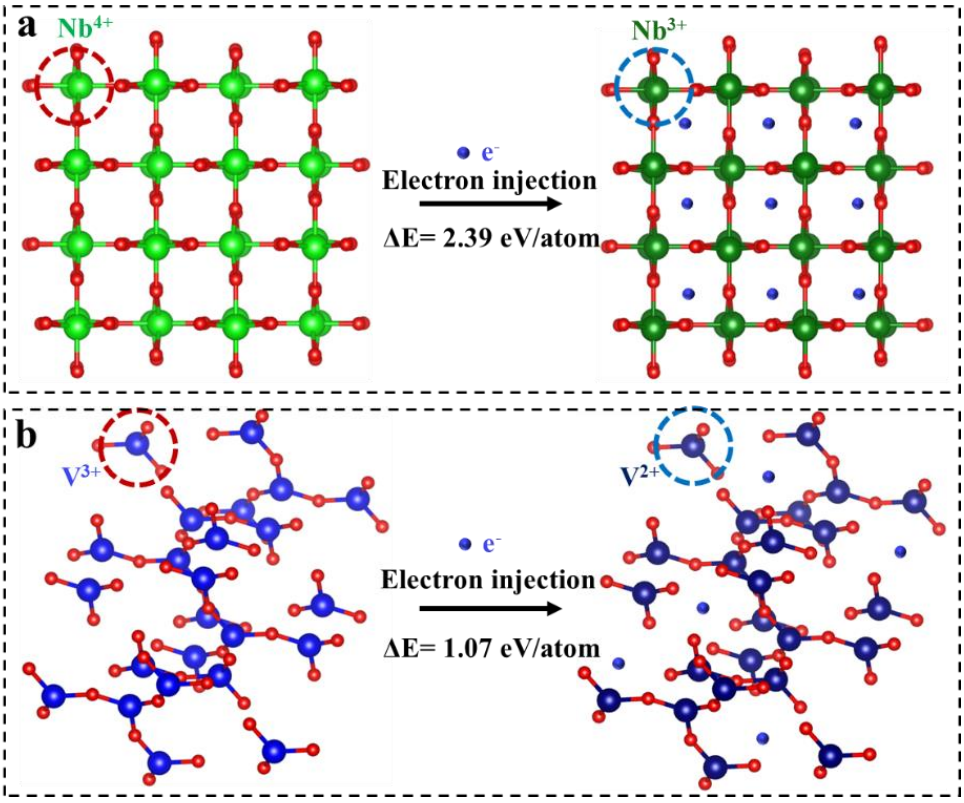


**Fig. S15 a** Energy changes in the $NbO_2$ model before and after electron injection. **b** Energy changes in the $V_2O_3$ model before and after electron injection

**Table S2** Li-Nb/Li-V atomic spacing in different models and overall energy difference (normalized based on model 1)

| | Model 1 | Model 2 | Model 3 | Model 4 |
|---|---|---|---|---|
| Li-Nb1 distance (Å) | 2.98 | 2.93 | 2.97 | 2.95 |
| Li-Nb2 distance (Å) | 2.74 | 4.84 | 4.89 | 4.86 |
| Li-Nb3 distance (Å) | 2.74 | 2.76 | 4.89 | 4.86 |
| Li-V1 distance (Å) | 2.47 | 2.48 | 2.47 | 2.47 |
| Li-V2 distance (Å) | 2.47 | 2.48 | 2.47 | 2.47 |
| Li-V3 distance (Å) | 3.86 | 3.55 | 3.55 | 3.56 |
| Li-V4 distance (Å) | 3.86 | 3.85 | 3.55 | 3.56 |
| Li-Nb average distance (Å) | 2.82 | 3.51 | 4.25 | 4.22 |
| Li-V average distance (Å) | 3.165 | 3.09 | 3.01 | 3.015 |
| ΔE(eV) | 0 | -0.19 | -0.4 | -3.9 |

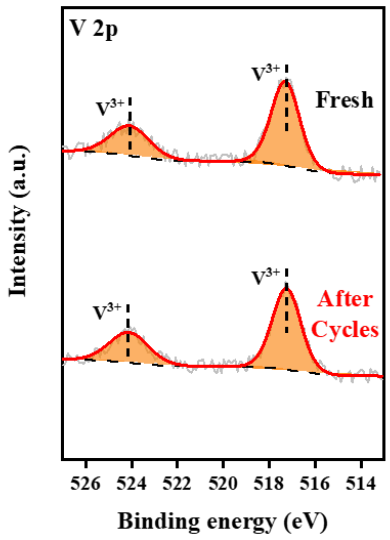


**Fig. S16** Post-mortem analysis of V 2p spectra of $VNbO_4$ after 1000 cycles

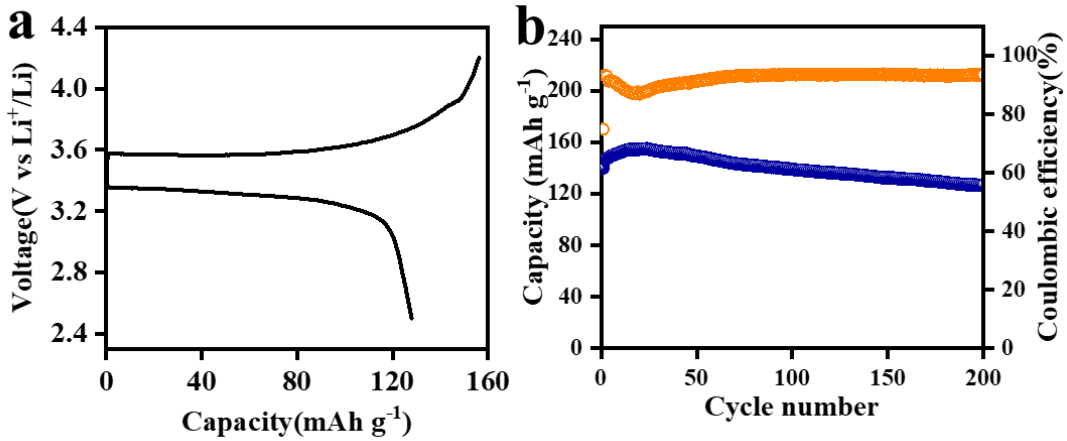


**Fig. S17 a** The initial charge-discharge curves of $LiFePO_4$@C at 1 C, **b** Cycle performance of $LiFePO_4$@C at 1 C

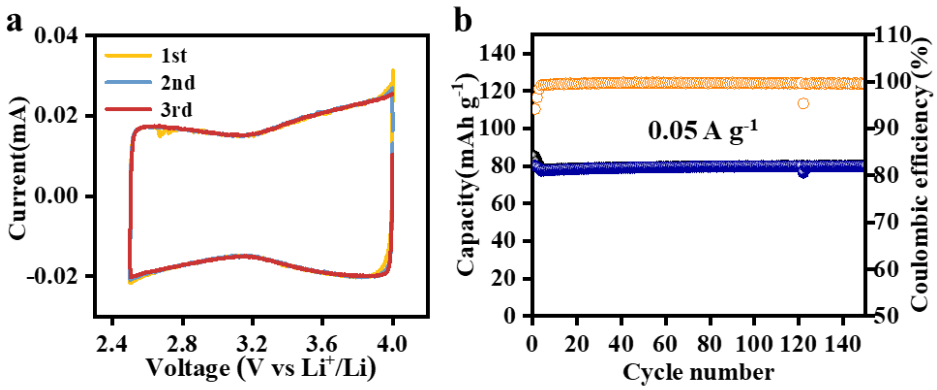


**Fig. S18 a** The initial three CV curves of AC, **b** Cycle performance of AC at 0.05 A $g^{-1}$.

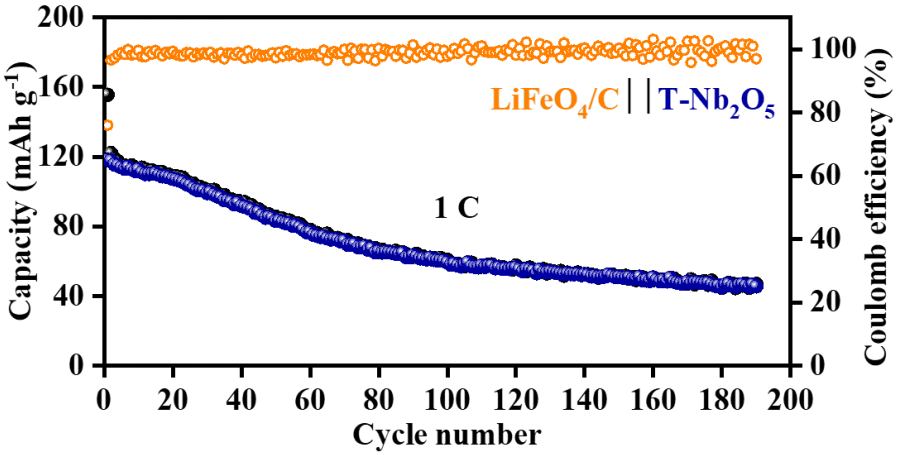


**Fig. S19** Cycle performance of $LiFePO_4$@C//T-$Nb_2O_5$ full cell at 1 C

## Supplementary References

[S1] K.J. Griffith, A.C. Forse, J.M. Griffin, C.P. Grey, High-rate intercalation without nanostructuring in metastable Nb2O5 bronze phases. J. Am. Chem. Soc. **138**, 8888 (2016). https://doi.org/10.1021/jacs.6b04345

[S2] S.F. Lou, X.Q. Cheng, L. Wang, J.L. Gao, Q. Li et al., High-rate capability of three-dimensionally ordered macroporous T-Nb2O5 through Li+ intercalation pseudocapacitance. J. Power Sources **361**, 80 (2017). https://doi.org/10.1016/j.jpowsour.2017.06.023

[S3] H.L. Yang, H.H. Xu, L.B. Wang, L. Zhang, Y.H. Huang et al., Microwave-assisted rapid synthesis of self-assembled T-Nb2O5 nanowires for high-energy hybrid supercapacitors. Chem. Eur. J. **23**, 4203 (2017). https://doi.org/10.1002/chem.201700010

[S4] J.M. Zhang, H. Chen, X.W. Sun, X.J. Kang, Y. Zhang et al., High intercalation

pseudocapacitance of free-standing T-Nb2O5 nanowires@carbon cloth hybrid supercapacitor electrodes. J. Electrochem. Soc. **164**, A820 (2017). https://doi.org/10.1149/2.1351704jes

[S5] X.D. Liu, G.Y. Liu, H. Chen, J.M. Ma, R.X. Zhang, Facile synthesis of Nb2O5 nanobelts assembled from nanorods and their applications in lithium ion batteries. J. Phys. Chem. Solids **111**, 8 (2017). https://doi.org/10.1016/j.jpcs.2017.07.007

[S6] D.P. Cao, Z.G. Yao, J.J. Liu, J.C. Zhang, C.L. Li, H-Nb2O5 wired by tetragonal tungsten bronze related domains as high-rate anode for Li-ion batteries. Energy Stor. Mater. **11**, 152 (2018). https://doi.org/10.1016/j.ensm.2017.10.005

[S7] B.H. Deng, T.Y. Lei, W.H. Zhu, L. Xiao, J.P. Liu, In-plane assembled orthorhombic Nb2O5 nanorod films with high-rate Li+ intercalation for high-performance flexible Li-ion capacitors. Adv. Funct. Mater. **28**, 1704330 (2018). https://doi.org/10.1002/adfm.201704330

[S8] Y.Z. Jiao, H.T. Zhang, H.L. Zhang, A. Liu, Y.X. Liu et al., Highly bonded T-Nb2O5/rGO nanohybrids for 4 V quasi-solid state asymmetric supercapacitors with improved electrochemical performance. Nano Res. **11**, 4673 (2018). https://doi.org/10.1007/s12274-018-2049-1

[S9] H.W. Chen, H.X. Zhang, Y.H. Wu, T. Zhang, Y.C. Guo et al., Nanostructured Nb2O5 cathode for high-performance lithium-ion battery with Super-P and graphene compound conductive agents. J. Electroanal. Chem. **827**, 112 (2018). https://doi.org/10.1016/j.jelechem.2018.08.037

[S10] H. Park, D. Lee, T. Song, High capacity monoclinic Nb2O5 and semiconducting NbO2 composite as high-power anode material for Li-Ion batteries. J. Power Sources **414**, 377 (2019). https://doi.org/10.1016/j.jpowsour.2019.01.015

[S11] J.H. Zhang, H.T. Zhang, Y.Q. Zhang, J.W. Zhang, H.Y. He et al., Unveiling of the energy storage mechanisms of multi -modified (Nb2O5@C)/rGO nanoarrays as anode for high voltage supercapacitors with formulated ionic liquid electrolytes. Electrochimica Acta **313**, 532 (2019). https://doi.org/10.1016/j.electacta.2019.04.160

[S12] X.Y. Han, P.A. Russo, N. Goubard-Bretesche, S. Patane, S. Santangelo et al., Exploiting the condensation reactions of acetophenone to engineer carbon-encapsulated Nb2O5 nanocrystals for high-performance Li and Na energy storage systems. Adv. Energy Mater. **9**, 1902813 (2019). https://doi.org/10.1002/aenm.201902813

[S13] S.D. Fu, Q. Yu, Z.H. Liu, P. Hu, Q. Chen et al., Yolk–shell Nb2O5 microspheres as intercalation pseudocapacitive anode materials for high-energy Li-ion capacitors. J. Mater. Chem. A **7**, 11234 (2019). https://doi.org/10.1039/C9TA02342A

[S14] S. Hemmati, G. Li, X.L. Wang, Y.L. Ding, Y. Pei et al., 3D N-doped hybrid architectures assembled from 0D T-Nb2O5 embedded in carbon microtubes toward high-rate Li-ion capacitors. Nano Energy **56**, 118 (2019). https://doi.org/10.1016/j.nanoen.2018.10.048

[S15] Q. Wang, Z.Y. Jia, L.G. Li, J. Wang, G.G. Xu et al., Coupling niobia nanorods with a multicomponent carbon network for high power lithium-ion batteries. Acs Appl. Mater. Interfaces **11**, 44196 (2019). https://doi.org/10.1021/acsami.9b14819

[S16] H.F. Yu, L. Xu, H.Y. Wang, H. Jiang, C.Z. Li, Nanochannel-confined synthesis of Nb2O5/CNTs nanopeapods for ultrastable lithium storage. Electrochimica Acta **295**, 829 (2019). https://doi.org/10.1016/j.electacta.2018.11.017

[S17] Z.H. Song, H. Li, W. Liu, H.Z. Zhang, J.W. Yan et al., Ultrafast and stable Li-(de)intercalation in a large single crystal H-Nb2O5 anode via optimizing the homogeneity of electron and ion transport. Adv. Mater. **32**, 2001001 (2020). https://doi.org/10.1002/adma.202001001

[S18] L. Qin, Y. Liu, S.Y. Xu, S.C. Wang, X. Sun et al., In-plane assembled single-crystalline T-Nb2O5 nanorods derived from few-layered Nb2CTx MXene nanosheets for advanced Li-ion capacitors. Small Methods **4**, 2000630 (2020). https://doi.org/10.1002/smtd.202000630

[S19] Z.Q. Hu, Q. He, Z. Liu, X. Liu, M.S. Qin et al., Facile formation of tetragonal-Nb2O5 microspheres for high-rate and stable lithium storage with high areal capacity. Sci. Bull. **65**, 1154 (2020). https://doi.org/10.1016/j.scib.2020.04.011

[S20] H.R. Li, D. Li, J. Shi, Z.Y. He, Z.C. Zhao et al., Carbon coated 3D Nb2O5 hollow nanospheres with superior performance as an anode for high energy Li-ion capacitors. Sustain. Energy Fuels **4**, 4868 (2020). https://doi.org/10.1039/D0SE00804D

[S21] D.W. Liang, L. Hu, L.L. Wang, L.L. Liu, S. Liang et al., Laser-assisted fabrication of pseudohexagonal phase niobium pentoxide nanopillars for lithium ion battery anodes. Chemnanomat **6**, 73 (2020). https://doi.org/10.1002/cnma.201900532

[S22] P.P. Jing, K.T. Liu, L. Soule, E.H. Wang, T.T. Li et al., Engineering the architecture and oxygen deficiency of T-Nb2O5-carbon-graphene composite for high-rate lithium-ion batteries. Nano Energy **89**, 106398 (2021). https://doi.org/10.1016/j.nanoen.2021.106398

[S23] Y. Chen, Z.Y. Pu, Y.B. Liu, Y.X. Shen, S.M. Liu et al., Enhancing the low-temperature performance in lithium ion batteries of Nb2O5 by combination of W doping and MXene addition. J. Power Sources **515**, 230601 (2021). https://doi.org/10.1016/j.jpowsour.2021.230601

[S24] M. Yang, S. Li, J.G. Huang, Three-dimensional cross-linked Nb2O5

polymorphs derived from cellulose substances: insights into the mechanisms of lithium storage. Acs Appl. Mater. Interfaces **13**, 39501 (2021). https://doi.org/10.1021/acsami.1c11720

[S25] Y.J. Zheng, Z.G. Yao, Z. Shadike, M. Lei, J.J. Liu et al., Defect-concentration-mediated T-Nb2O5 anodes for durable and fast-charging li-ion batteries. Adv. Funct. Mater. **32**, 2107060 (2022). https://doi.org/10.1002/adfm.202107060

[S26] F. Liu, Z. Zhu, Y.G. Chen, J.S. Meng, H. Wang et al., Dense T-Nb2O5/carbon microspheres for ultrafast-(dis)charge and high-loading lithium-ion batteries. Acs Appl. Mater. Interfaces **14**, 49865 (2022). https://doi.org/10.1021/acsami.2c15697

[S27] M.N. Liu, C. Yan, Y.G. Zhang, Separability criteria via sets of mutually unbiased measurements. Sci. Rep. **5**, 8326 (2015). https://doi.org/10.1038/srep13138

[S28] H. Kim, E. Lim, C. Jo, G. Yoon, J. Hwang et al., Ordered-mesoporous Nb2O5/carbon composite as a sodium insertion material. Nano Energy **16**, 62 (2015). https://doi.org/10.1016/j.nanoen.2015.05.015

[S29] X. Wang, C.Y. Yan, J. Yan, A. Sumboja, P.S. Lee, Orthorhombic niobium oxide nanowires for next generation hybrid supercapacitor device. Nano Energy **11**, 765 (2015). https://doi.org/10.1016/j.nanoen.2014.11.020

[S30] L. Wang, X. Zhang, C. Li, Y.N. Xu, Y.B. An et al., Cation-deficient T-Nb2O5/graphene Hybrids synthesized via chemical oxidative etching of MXene for advanced lithium-ion capacitors. Chem. Eng. J. **468**, 143507 (2023). https://doi.org/10.1016/j.cej.2023.143507

[S31] W. Fang, Y. Zhang, C. Kang, Q. Meng, A.R. Shi et al., Oxygen vacancies Nb2O5-x: Ultrastable lithium storage anode materials for advanced rechargeable batteries. Appl. Surf. Sci. **600**, 154068 (2022). https://doi.org/10.1016/j.apsusc.2022.154068

[S32] W.X. Zhang, P.C. Mao, Y.H. Jin, H. Ming, Z.P. Li et al., Oxygen-deficient polymorphic Nb2O5 micro/nanoscale three-dimensionally interconnected anodes with enhanced rate capability for lithium storage. J. Alloys Compd. **911**, 165064 (2022). https://doi.org/10.1016/j.jallcom.2022.165064

[S33] D.W. Kim, S.Y. Kim, K.S. Yang, Synthesis of freestanding binder- and additive-free carbon nanofiber with graphene-wrapped Nb2O5 composite anode for lithium-ion batteries. Nanotechnology **33**, 015602 (2022). https://doi.org/10.1088/1361-6528/ac162d

[S34] J. Lin, S.Y. Zhao, T.G. Tranter, Z.Y. Zhang, F. Peng et al., Modelling and experimental investigation of Nb2O5 as a high-rate battery anode material. Electrochimica Acta **443**, 141983 (2023). https://doi.org/10.1016/j.electacta.2023.141983

[S35] X.B. Ding, H.Y. Huang, Q.H. Huang, B.R. Hu, X.K. Li et al., Doping sites modulation of T-Nb2O5 to achieve ultrafast lithium storage. J. Energy Chem. **77**, 280 (2023). https://doi.org/10.1016/j.jechem.2022.10.049

[S36] G.Y. Liu, S.S. Liu, H. Chen, X.D. Liu, X.W. Luo et al., Highly [001]-oriented N-doped orthorhombic $Nb_2O_5$ microflowers with intercalation pseudocapacitance for lithium-ion storage. Nanoscale **14**, 11710 (2022). https://doi.org/10.1039/D2NR03187F

[S37] W.X. Zhang, P.X. Shen, L.Z. Qian, Y. Wang, H. Arandiyan et al., Nanoscale phase engineering in two-dimensional niobium pentoxide anodes toward excellent electrochemical lithium storage. Acs Appl. Energy Mater. **4**, 4551 (2021). https://doi.org/10.1021/acsaem.1c00186

[S38] T. Yang, Z.Z. Yang, X.F. Cheng, YH. Ding, Y.X. Fan et al., Three-dimensional hierarchical urchin-like Nb2O5 microspheres wrapped with N-doped carbon: An advanced anode for lithium-ion batteries. J. Alloys Compd. **876**, 160145 (2021). https://doi.org/10.1016/j.jallcom.2021.160145